Matching Medium Design for In-Body Communications Using Artificial Neural Networks

Cemre Cadir*, Omer A. Kati*, Sema Dumanli*,
*Electrical and Electronics Engineering Dept., Bogazici University, Istanbul, Turkey, sema.dumanli@boun.edu.tr

***Abstract*—Matching media are located between wearable antennas and the human body to enhance implant communications. The selection of the matching medium is a complicated problem, and there is yet no well-established approach. The simulations are computationally expensive, and the theoretical work is limited. Hence, this work proposes a novel approach by using artificial neural networks for determining the effect of various matching media. For this aim, a wearable repeater antenna, human tissue blocks with varying relative permittivities, and matching medium layer with varying relative permittivities and thicknesses are utilized. Employing more than 200 simulated designs, optimum matching medium designs are proposed, and the matching medium concept has been shown to increase the average transmitted power by 17.6%. Moreover, it is shown that the trained neural network model can predict the test cases with 4.5% mean error and the computational cost has been decreased by 91% compared to the empirical method.**

***Index Terms*—Wearable repeater antenna, matching medium, machine learning, artificial neural networks, implant communications.**

I. Introduction

Wearable antennas have gained more attention over the years for medical imaging [1], [2], diagnosis [3], treatment [4], and health monitoring [5] as well as for personal use. Wearable antenna design has its own challenges, and the main challenge is its proximity to a highly lossy object, the human body [6]. Due to its high water content, the human body absorbs electromagnetic energy, making implant communications harder. Due to the restrictions in transmit power of implant and wearable antennas, it is critical to minimize the losses associated with the in-body link. These losses are related to reflection, near-field loss, and path loss[7].

Matching medium, also referred to as bolus layer in the literature [4], aims to balance two types of these losses: Reflection and near-field loss. It spans most of the near field and shows transitional characteristics by preventing the abrupt change of electromagnetic properties from the antenna to the body. This idea has been applied for various cases, however, the matching media providing the best wave penetration are proposed without much explanation about its selection [8], [9]. An ultra-wideband spiral antenna is proposed for in-body communications and embedding the antenna in a matching medium having $\varepsilon_{\mathrm{r}} = 27$ is suggested [8]. In [9], a foam spacer is placed between the antenna and the phantom to increase the bandwidth.

There are a few studies focused on optimizing the matching medium. In [10], internal and external matching media for implanted antennas are investigated analytically, and it is proposed that the use of an external matching medium can decrease the power loss up to 7.9 dB. According to [11], when the matching medium is assumed to be of infinite size, the recommended relative permittivity for the matching medium should be lower than 20. However, [1] concentrates on matching, and recommends using a matching medium with a relative permittivity value close to the underlying tissue's. Many assumptions have to be made for theoretical work [12], and simulations take a myriad of computational power and time [13]. To the best of the authors' knowledge, there is yet no rule of thumb for optimum matching medium selection. This work brings a novel perspective by utilizing artificial neural networks (ANN) to determine the optimum matching medium.

Machine learning, of which popularity has been increasing rapidly, is being used for a variety of applications, and antenna design is not an exception. Machine learning and related techniques are advantageous thanks to their high speed [14]. In [15], an ANN that models reflectarray elementary components is proposed to optimize the design process, and this makes different phases of the antenna design numerically more efficient. Reference [16] uses an ANN to acquire the design values for optimizing the bandwidth of two bands of a monopole antenna, together with the other machine learning methods. As the new machine learning based antenna design techniques are established [17], [18], ANNs are being employed not only for antenna design [19], [20], but also for the inverse scattering problem, direction of arrival estimation and remote sensing [14]. It is suitable to use an ANN based approach to optimize the matching medium design, as the problem is well-defined, and its dependent and independent variables can be easily determined.

As pointed out in [19], the most significant problem of the machine learning applications in this field is building a data set that is sufficient to train the model. Hence, this work includes the steps for building the data set. The setup consists of a wearable repeater antenna conformed to body, an implantable antenna, and a matching medium layer, as seen in Fig. 1. The matching medium conductivity is taken as zero, and its relative permittivity and thickness are selected as independent variables. For the human tissue, namely the target tissue, relative permittivity is varied to represent different tissues, while all the other design variables are held constant. A measure of the power transmitted to the implanted antenna, which is in 1 cm depth, is calculated using Ansys High-Frequency Structure Simulator (HFSS) [21], along with the

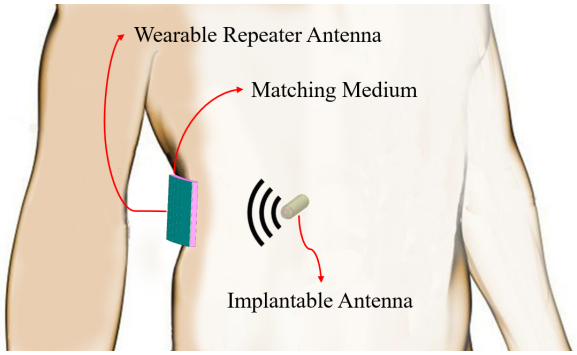

Fig. 1. Antenna conformed to body.

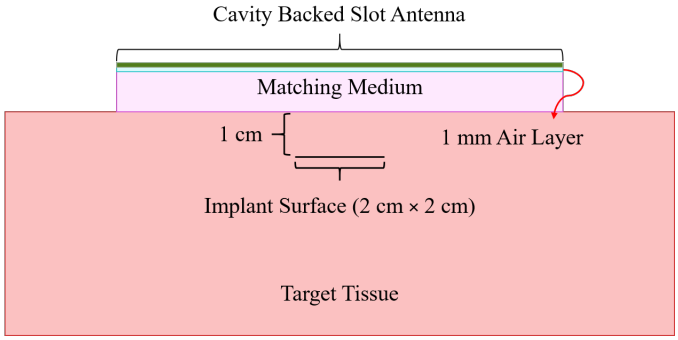

Fig. 2. The design of the cavity-backed slot antenna with the matching medium and target tissue.

S parameter characteristics in the 2.4 GHz ISM band. The trained model can replace the simulation tool for antenna design exploration and optimization in the established input space. Section II introduces the simulation setup, explains the data collection process, and demonstrates the simulation results. Section III establishes an ANN based approach, and illustrates the results. Section IV interprets the effect of matching medium, discussing the proposed approach. The paper concludes in Section V.

II. Empirical Work

A. Simulation Setup

Consider an HFSS design consisting of a cavity-backed slot antenna, a block of biological tissue representing the human body, and a matching medium between them, to be investigated later in this work, as depicted in Fig. 2. An air gap of 1 mm thickness is inserted between the antenna and the matching medium for better matching. The cavity-backed slot antenna is used as a wearable repeater establishing an in-body link with an implanted antenna. The implanted antenna is assumed to cover a square surface of area $4\ \mathrm{cm}^2$ in 1 cm depth.

Design variables can be classified into two categories: independent variables and control variables. The ranges of the independent variables can be seen in Table I. For ε_t = [20 40], ε_mm is swept with unit steps, and these samples are used for training and validation of the ANN. Remaining samples, which have ε_t = [30 50], are used for testing and their ε_mm is swept with five unit steps.

TABLE I
Values of Independent Variables

Features	Range
Relative permittivity of the matching medium (ε_mm)	[1:ε_t]
Thickness of the matching medium (d)	[9 14 19] mm
Relative permittivity of the target tissue (ε_t)	[20 30 40 50]

TABLE II
Dimensions of The Cavity-Backed Slot Antenna

Features	Value
Feed offset	0.75 cm
Width of target tissue (W_t)	15 cm
Length of target tissue (L_t)	20 cm
Slot width (W_slot)	6.3 cm
Slot length (L_slot)	0.05 cm
Substrate thickness (t_sub)	1 mm
Substrate width (W_sub)	7.5 cm
Substrate length (L_sub)	10 cm
Microstrip offset	2.3 cm
Microstrip width (W_ustrip)	2.37 mm

Control variables are kept constant and include the conductivity of the target tissue (σ_t), which is $1.71\,\mathrm{S/m}$, and the dimensions of the cavity-backed slot antenna, as seen in Table II. Throughout the simulations, the antenna model is kept unvaried. Hence, the results illustrate only the effect of the matching medium and the target tissue.

B. Automated Data Collection Process

After the simulation setups are determined, a matrix containing the design features is constructed in MATLAB environment. Then, parametric sweeps are automatically generated using a MATLAB script that embeds elements of the matrix in the HFSS script template.

Solution setup is configured before all optimetrics are analyzed. Two frequency sweeps are created, namely Far Field Sweep (FF_Sweep) and S-parameter Sweep (SParam_Sweep), to get the desired outputs. FF_Sweep is set to calculate the average power (P_avg) on the implant surface at 2.4 GHz. In addition, S-parameter sweep is set to extract values of $|S_{11}|$ at the resonant frequency (f_r) and at 2.4 GHz.

This time, after completion of simulations, MATLAB scripts are again used to generate data extraction scripts. Generated script extracts P_avg on implant surface by evaluating a fields calculator expression as follows: $/(Integrate(Surface(Rectangle1),\ Mag(Poynting)),$ $Integrate(Surface(Rectangle1), 1))$ Then, extracted output columns are appended to starting matrix in order to be used as the data set for the deep learning algorithm.

C. Results

The simulation results are examined, and optimum matching medium relative permittivities according to P_avg for various ε_t

TABLE III
THE EMPIRICALLY CALCULATED OPTIMUM MATCHING MEDIUM RELATIVE PERMITTIVITIES FOR CHANGING ε_t AND d VALUES

ε_t	ε_{mm}	d (mm)	P_{avg} (W/m^2)	$\lvert S_{11}\rvert$ at 2.4 GHz (dB)	f_r (GHz)	$\lvert S_{11}\rvert$ at f_r (dB)
20	16	9	1.52	-19.03	2.41	-19.10
20	11	14	1.26	-21.56	2.4	-21.56
20	20	19	1.05	-14.37	2.46	-16.01
30	20	9	1.92	-15.08	2.38	-15.16
30	10	14	1.56	-22.78	2.44	-32.78
30	25	19	1.45	-13.44	2.41	-13.44
40	19	9	2.37	-19.04	2.41	-19.14
40	13	14	2.09	-17.83	2.35	-19.53
40	27	19	1.69	-12.90	2.4	-12.90
50	20	9	2.76	-19.76	2.4	-19.76
50	15	14	2.29	-12.36	2.3	-14.78
50	30	19	1.91	-11.94	2.36	-12.30

and d values can be found in Table III. The resonant frequency of these designs are in the range of 2.35-2.46 GHz, and the $|S_{11}|$ values are in the desired range. It should be noted that results given in Table III for ε_t = [30 50] might not be the optimum values, as ε_{mm} is swept with five units instead of one unit. This issue is studied in Section III.

Comparing the cases with different d values, the optimum choice is found to be d = 9 mm, since it shows higher P_{avg} and better matching in all optimum designs. In addition to that, thinner matching media are favorable for wearable applications considering user acceptance.

III. NEURAL NETWORK BASED APPROACH

A. Data Set

The data set is divided into three parts as training, validation and test sets. As mentioned in Section II, the training and validation sets consist of data samples with ε_t = [20 40], whereas test set consists of data samples having ε_t = [30 50]. Training and validation sets are split randomly such that ratio between them is 4:1. The number of samples for training, validation and test sets are 134, 34, and 47, respectively.

Neural network has three input variables (ε_{mm}, d, and ε_t) and four output variables. The output variables are P_{avg} and $|S_{11}|$ at 2.4 GHz together with f_r and $|S_{11}|$ at f_r. All input and output variables are normalized (i.e. divided by the maximum absolute values) for faster training.

B. Neural Network Structure

The neural network is realized using Keras and consists of an input layer, nine hidden layers, a dropout layer, and an output layer, as seen in Fig. 3. Each of the hidden layers has nine neurons, while the output layer has four neurons. For regularization, the dropout rate is chosen to be 0.1. That means each neuron has a dropout chance of 10% in each epoch of the training. A maximum norm constraint of 3 is utilized for each neuron.

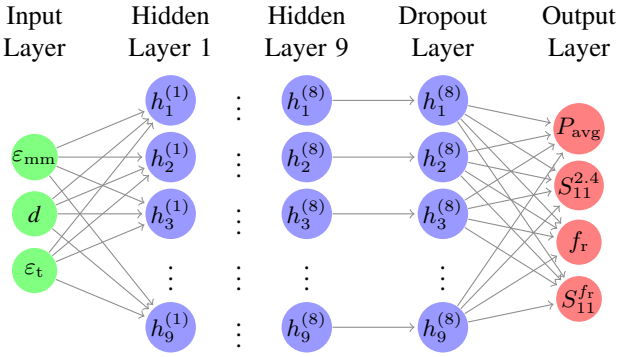

Fig. 3. ANN diagram for matching medium optimization.

Adam optimization and mean absolute percentage error (MAPE) loss function are selected. Keras default settings are used for both Adam optimization and MAPE calculation. In addition to MAPE, Mean Absolute Error (MAE) is monitored for training and validation sets.

C. Training

For training, the batch size is chosen as 32, and it corresponds to 5 batches per epoch. The model is trained for ten thousand epochs, and the best performing model in terms of MAE and MAPE on the validation set is restored at the end of the training with an early stopping function. By using this technique, the end model has been trained for 9707 epochs.

D. Results

TABLE IV
MAPE AND STD VALUES FOR THE ANN MODEL IN TERMS OF DIFFERENT DATA CATEGORIES

	Training		*Validation*		$\varepsilon_t = 30$		$\varepsilon_t = 50$	
	MAPE	STD	MAPE	STD	MAPE	STD	MAPE	STD
$d = 9mm$								
P_{avg}	2.331	1.52	1.978	1.35	1.569	1.68	7.126	2.81
$S_{11}^{2.4}$	3.196	2.16	2.980	1.55	5.033	2.55	5.695	3.96
f_r	0.691	0.47	0.554	0.44	0.739	0.62	1.161	0.95
$S_{11}^{f_r}$	3.940	4.64	4.758	6.49	2.552	2.38	6.637	4.81
$d = 14mm$								
P_{avg}	2.388	1.71	1.665	1.43	2.612	1.24	4.958	3.5
$S_{11}^{2.4}$	3.502	5.29	3.475	3.82	5.480	2.77	11.117	10.68
f_r	0.860	0.75	0.853	0.66	0.752	0.92	1.834	1.41
$S_{11}^{f_r}$	3.909	7.29	2.228	1.59	3.834	3.16	5.645	4.91
$d = 19mm$								
P_{avg}	3.052	3.69	3.707	5.73	5.778	5.77	7.403	4.64
$S_{11}^{2.4}$	3.362	4.00	2.381	1.57	4.191	3.83	4.794	5.59
f_r	1.072	1.19	1.108	0.77	1.628	1.58	1.994	1.81
$S_{11}^{f_r}$	3.355	5.32	2.526	1.84	2.823	2.99	6.166	3.55

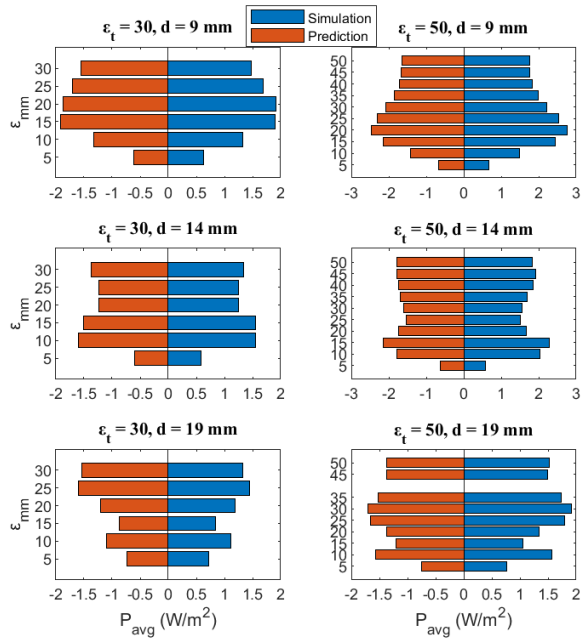

Fig. 4. Comparison of P_{avg} between Predictions and Simulation Results

The predictions for the outputs are obtained using the trained model. MAPE is calculated and categorized by ε_{t} and d values as seen in Table IV. The standard deviation (STD) of the absolute percentage errors for the samples is also provided. The overall MAPE values for the training, validation, and test sets are 2.6377, 2.3053, and 4.5048, respectively. It can be seen that all MAPE values are below 7.4%, except for the $|S_{11}|$ at 2.4 GHz of the $\varepsilon_{\text{t}} = 50$ and d=14 mm. This relatively high MAPE value can be compensated for by looking at other two outputs, f_{r} and $|S_{11}|$ at f_{r}, which have lower MAPE.

In Fig. 4, P_{avg} of all the test set samples can be seen. The simulated and predicted values are given side by side for easy comparison. The optimum ε_{mm} values for ε_{t} = [30 50] and d = [9 14 19] mm can be read from Fig. 4.

For the input space overlapping the test set, the predictions are obtained with steps of one unit, and the optimum matching medium predictions for each case are provided in Table V. Then, simulations for these optimum designs are run using HFSS, and simulation results are also found in Table V.

When Table III and Table V are viewed together, it is obvious that the predictions offer a refinement on the optimum designs except for two cases. The optimum design prediction for ε_{t} = 50, d = 9 mm stayed the same as in the simulation results. For the case having ε_{t} = 30 and d = 19 mm, the optimum is falsely predicted with 1.4% decrease in the P_{avg} compared to the previous results. Even if the $|S_{11}|$ predictions are not exactly true, all of them are in the desired range. Despite the exceptional errors, the ANN based approach seems promising considering the time needed for the empirical study.

TABLE V
COMPARISON OF BEST ANN PREDICTIONS AND THEIR HFSS SIMULATION COUNTERPARTS FOR THE TEST SET

ε_{t}	ε_{mm}	d (mm)	P_{avg} (W/m^2)	$\lvert S_{11}\rvert$ at 2.4 GHz (dB)	f_{r} (GHz)	$\lvert S_{11}\rvert$ at f_{r} (dB)
ANN Predictions						
30	17	9	1.96	-18.44	2.41	-19.67
30	12	14	1.73	-18.54	2.36	-19.57
30	27	19	1.62	-12.10	2.43	-12.48
50	20	9	2.46	-18.64	2.39	-17.98
50	13	14	2.26	-21.35	2.37	-23.16
50	28	19	1.73	-12.56	2.43	-12.39
Simulation Results						
30	17	9	1.97	-19.76	2.40	-19.76
30	12	14	1.70	-12.04	2.37	-12.17
30	27	19	1.43	-13.29	2.39	-13.35
50	20	9	2.76	-20.44	2.38	-21.00
50	13	14	2.45	-18.08	2.35	-22.49
50	28	19	1.93	-19.27	2.43	-19.91

TABLE VI
SIMULATION RESULTS OF THE DESIGNS WITH ONLY 1 MM AIR LAYER

ε_{t}	d (mm)	P_{avg} (W/m^2)	$\lvert S_{11}\rvert$ at 2.4 GHz (dB)	f_{r} (GHz)	$\lvert S_{11}\rvert$ at f_{r} (dB)
20	0	1.35	-9.72	2.52	-10.87
30	0	1.73	-9.38	2.49	-9.91
40	0	2.01	-8.89	2.47	-9.17
50	0	2.19	-8.27	2.48	-8.60

IV. DISCUSSION

In the data set used to train the model, the distances between the antenna and the target tissue vary as 1, 1.5, and 2 cm, including a 1 mm air layer. For the cases corresponding to these thicknesses and targeting different tissues, the matching medium was replaced with the air layer of the same thickness. When the simulation results were averaged, it was noted that the average received power was 0.1006 W/m2, $|S_{11}|$ was 0.9308 dB at 2.4 GHz, and there was a shift of more than 0.3 GHz at the resonance frequency. From these simulation results, the effect of replacing the matching medium with the air layer can be seen, provided that the distance of the antenna to the target tissue remains constant.

Besides, the cases where the matching medium was eliminated (i.e. only 1 mm air layer is left between the antenna and the tissue block) were simulated, and the results can be seen in Table VI. From these results, it can be seen that P_{avg} can be increased by introducing a matching medium without significantly affecting the remaining outputs. Investigating Table III and Table V, the best average power levels for each ε_{mm} are achieved with d = 9 mm matching media. When those

designs are considered together with the designs in Table VI, it can be calculated that the matching medium increases P_{avg} by 17.6% on average. With these results, the importance of matching medium optimization using ANNs is demonstrated.

The empirical method can be compared with the ANN approach in terms of the computational cost. With the empirical method, around 2400 different models (for ε_{t} = [30:1:50], $\varepsilon_{\mathrm{mm}}$ = [1:1:ε_{t}], and d = [9 14 19] mm) should be simulated to cover the established input space. Considering that one simulation takes 35 minutes in average, completing the simulations would take around 1400 hours. Utilizing our ANN approach, the time needed for covering the same space has been reduced to 125 hours, which correspond to 215 simulations. Training the ANN and obtaining the predictions take less than 5 minutes. It can be concluded that using ANN is an effective way of optimization.

V. Conclusion

Forming a reliable in-body link is a challenging task due to the high relative permittivity and lossy nature of human tissues. The wearable and the implantable antenna are subject to near-field losses if faced directly with these tissues. Also, EM waves transmitted by the wearable antenna undergo reflection at the air-skin interface. The use of a matching medium can minimize the reflection and the near-field losses associated with the wearable antenna. Here, it has been shown that the use of an optimum matching medium does not only maximize the average received power by the implant antenna but also stabilizes the response of the wearable antenna eliminating detuning. The search for this optimum medium is achieved by using an ANN, significantly lowering the computational cost.

In the future, the input space will be expanded by widening the ranges of current independent variables and adding new independent variables such as σ_{t}, depth of the implanted antenna, and the frequency band. Various electrical and magnetic antennas will be investigated. Since the problem will become more complicated in those future large-scale studies, the role and importance of ANN will be more preeminent than that of this work.

Acknowledgment

This study is financially supported by Boğaziçi University Research Fund under project number 14543.

References

[1] F. Wang and T. Arslan, "Body-coupled monopole UWB antenna for wearable medical microwave imaging applications," 2017 IEEE-APS Topical Conference on Antennas and Propagation in Wireless Communications (APWC), Verona, 2017.

[2] Molaei, Ali Ghanbarzadeh, Ashkan Heredia-Juesas, Juan Martinez, Jose. (2015). Miniaturized UWB Antipodal Vivaldi Antenna for a mechatronic breast cancer imaging system.

[3] A. S. M. Alqadami, K. S. Bialkowski, A. T. Mobashsher and A. M. Abbosh, "Wearable Electromagnetic Head Imaging System Using Flexible Wideband Antenna Array Based on Polymer Technology for Brain Stroke Diagnosis," in IEEE Transactions on Biomedical Circuits and Systems, vol. 13, no. 1, pp. 124-134, Feb. 2019.

[4] Singh, Soni Sahu, Bhagirath Singh, Surya Pal. (2017). Hyperthermia performance of conformal applicator for limb tumor in presence of water bolus.

[5] T. Huong Nguyen, T. Lan Huong Nguyen and T. Phu Vuong, "A Printed Wearable Dual Band Antenna for Remote Healthcare Monitoring Device," 2019 IEEE-RIVF International Conference on Computing and Communication Technologies (RIVF), Danang, Vietnam, 2019.

[6] S. Dumanli, "Challenges of wearable antenna design," 2016 11th European Microwave Integrated Circuits Conference (EuMIC), London, 2016.

[7] C. A., Balanis, Antenna Theory: Analysis and Design. New York, NY, USA: Wiley, 1997.

[8] Khaleghi, Ali Balasingham, Ilangko Chávez-Santiago, Raúl. (2014). An ultra-wideband wire spiral antenna for in-body communications using different material matching layers. 2014 36th Annual International Conference of the IEEE Engineering in Medicine and Biology Society, EMBC 2014. 2014.

[9] G. A. Conway and W. G. Scanlon, "Antennas for Over-Body-Surface Communication at 2.45 GHz," in IEEE Transactions on Antennas and Propagation, vol. 57, no. 4, pp. 844-855, April 2009.

[10] F. Merli, B. Fuchs, J. R. Mosig and A. K. Skrivervik, "The Effect of Insulating Layers on the Performance of Implanted Antennas," in IEEE Transactions on Antennas and Propagation, vol. 59, no. 1, pp. 21-31, Jan. 2011.

[11] Chávez-Santiago, Raúl Khaleghi, Ali Balasingham, Ilangko. (2014). Matching layer for path loss reduction in ultra wideband implant communications. 2014 36th Annual International Conference of the IEEE Engineering in Medicine and Biology Society, EMBC 2014. 2014. 6989-92.

[12] Rappaport, C.M.. (2008). Determination of Bolus Dielectric Constant for Optimum Coupling of Microwaves through Skin for Breast Cancer Imaging. International Journal of Antennas and Propagation. 2008.

[13] Angiulli, Giovanni De Carlo, Domenico Isernia, T.. (2013). A sensitivity study for microwave breast cancer detection using the Contrast-Source Integral Equation and realistic anthropomorphic numerical 3-D phantoms. International Journal of Applied Electromagnetics and Mechanics. 43.

[14] A. Massa, D. Marcantonio, X. Chen, M. Li and M. Salucci, "DNNs as Applied to Electromagnetics, Antennas, and Propagation—A Review," in IEEE Antennas and Wireless Propagation Letters, vol. 18, no. 11, pp. 2225-2229, Nov. 2019.

[15] Freni, A. Mussetta, Marco Pirinoli, Paola. (2012). Neural Network Characterization of Reflectarray Antennas. International Journal of Antennas and Propagation. 2012.

[16] Y. Sharma, H. H. Zhang and H. Xin, "Machine Learning Techniques for Optimizing Design of Double T-Shaped Monopole Antenna," in IEEE Transactions on Antennas and Propagation, vol. 68, no. 7, pp. 5658-5663, July 2020.

[17] A. D. Boursianis, S. Koulouridis, D. Georgoulas and S. K. Goudos, "Wearable 5-Gigahertz Wi-Fi Antenna Design Using Whale Optimization Algorithm," 2020 14th European Conference on Antennas and Propagation (EuCAP), Copenhagen, Denmark, 2020.

[18] M. O. Akinsolu, K. K. Mistry, B. Liu, P. I. Lazaridis and P. Excell, "Machine Learning-assisted Antenna Design optimization: A Review and the State-of-the-art," 2020 14th European Conference on Antennas and Propagation (EuCAP), Copenhagen, Denmark, 2020.

[19] C. Maeurer, P. Futter and G. Gampala, "Antenna Design Exploration and Optimization using Machine Learning," 2020 14th European Conference on Antennas and Propagation (EuCAP), Copenhagen, Denmark, 2020.

[20] J. Tak, A. Kantemur, Y. Sharma and H. Xin, "A 3-D-Printed W-Band Slotted Waveguide Array Antenna Optimized Using Machine Learning," in IEEE Antennas and Wireless Propagation Letters, vol. 17, no. 11, pp. 2008-2012, Nov. 2018.

[21] ANSYS HFSS: High Frequency Electromagnetic Field Simulation Software. [Online]. Available: https://www.ansys.com/products/electronics/ansys-hfss. [Accessed: 15-Oct-2020].